Dominant harmonic pattern as an ictal marker of the epileptogenic zone in focal neocortical epilepsy

Lingqi Ye[1, 2, 3], Lingli Hu[1], Hongyi Ye[1], Yihe Chen[1], Junming Zhu[2, 4], Zhe Zheng[4], Hongjie Jiang[4], Dongping Yang[5], Cong Chen[1], Shan Wang[1], Zhongjin Wang[1], Wenjie Ming[1], Yi Wang[6], Cenglin Xu[6], Jin Wang[3], Meiping Ding[1], Shuang Wang[1, 2]*

1. Department of Neurology and Epilepsy Center, Second Affiliated Hospital, School of Medicine, Zhejiang University, Hangzhou, China
2. Nanhu Brain-computer Interface Institute, Hangzhou, China
3. Department of Neurology, Sir Run Run Shaw Hospital, School of Medicine, Zhejiang University, Hangzhou, China
4. Department of Neurosurgery, Second Affiliated Hospital, School of Medicine, Zhejiang University, Hangzhou, China
5. Research Center for Augmented Intelligence, Research Institute of Artificial Intelligence, Zhejiang Lab, Hangzhou, China
6. Key Laboratory of Neuropharmacology and Translational Medicine of Zhejiang Province, School of Pharmaceutical Sciences, Zhejiang Chinese Medical University, Hangzhou, China

*Correspondence to：

Shuang Wang*, Department of Neurology, Second Affiliated Hospital, School of Medicine, Zhejiang University, Hangzhou 310009, China; Tel: +86-571-87783872; E-mail: wangs77@zju.edu.cn

Abstract

Objective: The ictal *Harmonic* pattern (*H* pattern), produced by the non-linear characteristics of EEG waveforms, may hold significant potential for localizing the epileptogenic zone (EZ) in focal epilepsy. However, further validation is needed to establish the *H* pattern's effectiveness as a biomarker for measuring the EZ.

Methods: We retrospectively enrolled 131 patients diagnosed with drug-resistant focal epilepsy, all of whom had complete stereo-electroencephalographic (SEEG) data. From this cohort, we selected 85 patients for outcome analysis. We analyzed the morphological and time-frequency (TF) features of the *H* pattern using TF plots. A third quartile (Q3) threshold was applied to classify channels expressing either dominant ($Channel_{dH\ pattern}$) or non-dominant *H* patterns ($Channel_{non\text{-}dH\ pattern}$). We then examined associations between the morphological features of the *H* pattern and patients' clinical characteristics, as well as the correlations between the extent of channel removal and seizure outcomes.

Results: We found no significant correlations between the morphological features of the ictal *H* pattern and clinical factors, including lesional MRI findings, epileptic onset patterns, epilepsy type, pathology, or surgical outcomes. The non-localizable *H* pattern appeared exclusively in patients with non-focal onset patterns. Notably, the proportion of $Channel_{dH\ pattern}$ was higher in the seizure-onset zone (SOZ) compared to the early propagation zone. The seizure-free group demonstrated significantly higher removal proportions of $Channel_{dH\ pattern}$, both within and outside the SOZ (p = 0.014; p = 0.036), with AUCs of 0.606 and 0.660, respectively, in a seizure freedom prediction model. Survival analysis confirmed that complete removal of these regions correlated with long-term seizure freedom (p = 0.008; p = 0.028). Further subgroup analysis showed a significant correlation in neocortical epilepsy (p = 0.0004; p = 0.011), but not in mesial temporal lobe epilepsy. Additionally, multivariate analysis identified the complete removal of $Channel_{dH\ pattern}$ as the only independent predictor for seizure freedom (p = 0.022; OR 6.035, 95% CI 1.291-28.211).

Conclusions: Our study supports the notion that the dominance of the ictal *H* pattern,

regardless of its morphology, serves as a novel biomarker for the EZ in focal epilepsy. The non-linearity in EEG waveforms provides new insights into understanding ictal spreading propagation and offers potential improvements for surgical planning in neocortical epilepsy.

Keywords: harmonic pattern; focal epilepsy; epileptogenic zone; epilepsy surgery; seizure outcome

Introduction

Resective surgery currently remains the most effective treatment for drug-resistant epilepsy (DRE). However, only 50% of patients achieve prolonged seizure freedom following surgery. Despite advancements in intracranial electroencephalography (iEEG) technology, it has yet to surpass a 70% ceiling in achieving favorable surgical outcomes [1-3]. The success of the surgery largely depends on the precise localization and complete removal of the epileptogenic zone (EZ), which is defined as the brain area essential for generating seizures [4]. Postsurgical seizure freedom indicates that the EZ was likely successfully removed. Although the seizure-onset zone (SOZ) does not necessarily equate to the EZ [5, 6], experienced clinicians' visual identification of the SOZ is a crucial step in the process of localizing the EZ.

Many studies have aimed to identify ictal EEG biomarkers capable of quantitatively delineating the EZ. Established semi-quantitative algorithms, such as the epileptogenic index (EI) [7] and epileptogenic map [8], have been shown to be effective in cases where ictal onset patterns include low-voltage fast activity. Additionally, the removal of areas exhibiting ictal high-frequency oscillations (HFOs) has been reported as a prognostic indicator of favorable seizure outcomes [9-11]. The concept of the EEG *fingerprint*, proposed as an ictal biomarker of the EZ, suggests a possible synchronous activation of GABAergic neurons at seizure onset [12]. Similarly, *brain chirp* [13] highlights the importance of fast EEG activity in defining the EZ.

In our previous study, we identified the *Harmonic* pattern (*H* pattern), a spectral feature of specific ictal EEG components that contains valuable information for seizure propagation and EZ localization. The *H* pattern is characterized by an equidistant spectral band distribution of varying frequencies on time-frequency (TF) plots. Generated by the specific non-sinusoidal waveforms, the ictal *H* pattern may represent periodically synchronized neural firings, rather than a methodological artifact. Furthermore, the *H* pattern is frequently observed in seizures with various onset patterns and across different seizure stages [14]. The dominance of the ictal *H*

pattern in different brain regions reflects higher non-linearity and has proven useful in localizing the EZ.

Despite its potential, the full spectrum of the ictal *H* pattern remains unclear. The *H* pattern shows significant variability in morphology across patients; however, within an individual patient, its morphology and spatial localization tend to remain consistent across seizures, emphasizing the personalized nature of ictal neural dynamics. In this expanded cohort, we first investigated clinical factors related to the morphological properties of the *H* pattern, specifically focusing on its clarity and shape. High clarity indicates a narrower frequency band with reduced background noise, while the shape of the spectral bands reflects changes in the frequency of ictal neural oscillations at a macroscopic level. This study aims to further support the hypothesis that the dominance of the ictal *H* pattern could serve as a novel biomarker for the EZ. Additionally, we analyzed the potential impact of the *H* pattern's morphological features.

Methods

Selection of patient cohort

We retrospectively reviewed 133 patients with drug-resistant epilepsy who had completed stereo-electroencephalography (SEEG) at the Second Affiliated Hospital Zhejiang University School of Medicine (SAHZU) between April 2013 and October 2022. We excluded two patients diagnosed with hypothalamic hamartoma from the study. Therefore, we performed *H* pattern analysis on the remaining 131 cases. From this cohort, we selected 85 patients for outcome analysis based on the following inclusion criteria (**Figure S1**): (1) a focal-onset pattern on SEEG with a clearly defined SOZ localized to a discrete cortical region; (2) undergoing either resective surgery or thermocoagulation treatment; (3) recording at least two habitual clinical seizures during SEEG monitoring; (4) identifying a discernible and localizable ictal *H* pattern (as described in the *Identification of ictal H pattern* section); (5) a follow-up

116 period of at least 12 months after surgery. The Medical Ethics Committee of SAHZU
117 approved this study (Study No. 2023-1260, 2021-0585). We obtained written
118 informed consent from each participant.

119

120 ***SEEG evaluation***

121 All patients were recommended for SEEG evaluation during a multidisciplinary
122 patient management conference. The non-invasive presurgical evaluation included a
123 detailed medical history, neuropsychological assessment, scalp video-EEG
124 monitoring, 3.0-Tesla cerebral MRI, and interictal ^{18}F-fluorodeoxyglucose positron
125 emission tomography (^{18}F-FDG-PET). The procedure for SEEG electrode
126 implantation has been previously described [15]. Based on the working hypothesis,
127 multiple-contact intracerebral electrodes (8-16 contacts, each 2 mm in length, 0.8 mm
128 in diameter, and spaced 1.5 mm apart) were implanted using a robotic arm-assisted
129 system. SEEG signals were recorded at sampling rates of either 1,000 or 2,000 Hz
130 using EEG systems with 256 channels (Nihon Kohden) or 128 channels (Xltek,
131 Natus). The anatomical locations of each contact along the electrode trajectory in all
132 subjects were confirmed by co-registering post-implantation CT scans with
133 pre-implantation MRI using *Sinovation 2.0* [16]. A three-dimensional schematic
134 diagram of the reconstruction is provided in the flowchart (**Figure 1C**).

135

136 ***Surgical outcome***

137 Following SEEG evaluation, patients underwent either resective surgery or laser
138 ablation. The planning of these surgical interventions was conducted independently of
139 this study. Each contact was classified as either *removed* or *non-removed* based on
140 postsurgical MRI evaluations. Surgical outcomes were assessed at the most recent
141 follow-up and patients were categorized as either seizure-free (SF, Engel class Ia) or
142 not seizure-free (NSF, >Engel class Ia) [17].

Visual EEG analysis

Two experienced and board-certified neurophysiologists reviewed the SEEG data to identify the SOZ and the rapid propagation zone (PZ) using our previously established methods [15, 18]. The SOZ is defined as the brain area that shows the earliest changes on SEEG. The PZ is characterized by the rapid spread of ictal activity within 3-5 seconds after seizure onset. Areas outside these defined zones were classified as 'other regions.' Both the PZ and these 'other regions' were collectively categorized as non-SOZ.

Identification of ictal H pattern

We selected only contacts within cortical gray matter for quantitative analysis. We analyzed all EEG data using a bipolar montage. For each identified seizure, we extracted a 110-second segment of SEEG data: 10 seconds before and 100 seconds after the EEG onset. Additionally, we collected a segment of preictal EEG data ranging from -230 to -120 seconds before EEG onset as baseline data for normalization. To enhance the reliability of our results, we applied two analytical methods: the Morlet wavelet transform[19] and the multitaper method [20, 21] in the TF analysis.

We identified the ictal *H* pattern from TF maps based on the following criteria: the presence of two or more distinct high-intensity bands with varying frequencies occurring at any point during a seizure, with equal frequency intervals between adjacent bands (**Figure 1A**). For each patient, we analyzed only the initially occurring *H* pattern. We estimated various features of the ictal *H* pattern, including its shape, clarity, onset and end times, fundamental and maximal frequencies, frequency intervals, and the number of bands. If the *H* pattern was consistently stereotyped across different seizures for a single patient, we included only one data set in the analysis. To determine the dominance of the *H* pattern, we established a threshold

known as *Q3*, which represents the upper quartile (75th percentile) of the data distribution for the maximal count of frequency bands per patient. We calculated *Q3* using the following formula:

$$Q3 = (n + 1) * 3/4\,,$$

where *n* denotes the highest count of frequency bands observed across all channels. If the number of bands in a channel showing the ictal *H* pattern ($Channel_{H\ pattern}$) exceeds the *Q3* threshold, we marked it as exhibiting a dominant *H* pattern ($Channel_{dH\ pattern}$). Conversely, a channel not meeting this threshold was classified as expressing a non-dominant *H* pattern ($Channel_{non\text{-}dH\ pattern}$) (**Figure 1D**). A localizable *H* pattern should be consistent across seizures and present in specific regions. If no gradient in band numbers was observed across all channels, the *H* pattern was classified as non-localizable.

Morphology of Ictal Harmonic Pattern

We classified the clarity of the *H* pattern into two levels. Grade A indicated a highly clear frequency band with distinct borders against the background activity. Grade B referred to a less clear frequency band with fuzzier borders. We identified three distinct shapes of the *H* pattern: Shape 1 resembled a parabola, where the fundamental frequency initially increases and then decreases; Shape 2 appeared as a declining line, representing a decrease in the frequency harmonics of the spectral band; and Shape 3 took the form of an ascending line, indicating an increase in the frequency harmonics of the spectral band. This resulted in a total of six categories: A1, A2, A3, B1, B2, and B3 (**Figure S2**). Initially, two investigators (Ye L.Q. and Hu L.L.) performed these classifications. In cases of disagreement, a third epileptologist (Wang S.) made the final decision.

Prediction of Surgical Outcome

For each patient, we categorized channels as either SOZ or non-SOZ based on visual

199 analysis, and as $Channel_{dH\ pattern}$ or $Channel_{non\text{-}dH\ pattern}$ based on TF analysis. We
200 determined the ratio of removed channels using the following formula:

$$Removal\ ratio(\%) = \frac{\#Channel_{removed}}{\#Channel_{removed} + \#Channel_{non-removed}} \times 100\%.$$

201 To estimate the correlation between the removal of $Channel_{dH\ pattern}$ and seizure
202 freedom, we used the *Chi-Squared* test and receiver operating characteristic (ROC)
203 curve analysis, from which we derived the area under the curve (AUC). We then
204 generated Kaplan-Meier (KM) curves to depict the cumulative probability of
205 achieving seizure freedom. We compared the retention of seizure freedom between
206 groups using the log-rank test, including patients with complete (100%) removal and
207 those with incomplete or no removal (0-100%).

208

209 **Statistical Analysis**

210 We used MATLAB 2021a (The MathWorks, Inc.) and SPSS 26.0 for statistical
211 analysis. We evaluated the normality of the distribution of all continuous variables
212 using the *Kolmogorov-Smirnov* test. Normally distributed variables were presented as
213 mean ± standard deviation (SD), while non-normally distributed variables were
214 reported as median (interquartile range, IQR). We expressed categorical variables as
215 frequencies. We applied an *unpaired t*-test or a nonparametric *Mann-Whitney U* test
216 to analyze continuous variables, and we assessed categorical variables using the
217 *Chi-Squared* test. We also conducted a binary regression analysis to identify
218 predictive factors affecting surgical outcomes. For multiple comparisons, we
219 employed the Bonferroni correction method. $p < 0.05$ represents statistically
220 significant.

221

222 **Results**

223 ***Patient Demographics***

224 In the entire cohort, 75.6% (99 patients) exhibited a focal-onset pattern, while the

remaining 24.4% (32 patients) had a non-focal onset pattern (**Table S1**). Among those with a focal-onset pattern, 92.9% (92 patients) displayed an ictal *H* pattern, all of which were localizable. In contrast, 93.8% (30 patients) of those with a non-focal onset pattern exhibited at least one ictal *H* pattern. Of these, 80.0% (24 patients) were localizable, and 20.0% (6 patients) were non-localizable. Most patients presented with only one type of *H* pattern. However, two different types of *H* pattern were observed exclusively in approximately 20% of patients with a non-focal onset pattern (**Table S1**).

Of the 85 patients included in the outcome analysis, 38.9% (33 patients) had participated in our previous *H* pattern study (**Table 1**) [14]. In the current cohort, 61.2% (52 patients) achieved seizure freedom after an average follow-up period of 47.8 months. We found no significant differences between the SF and NSF groups regarding age at disease onset, age at SEEG recording, or the lateralization/localization of seizures. The incidence of detectable abnormalities on MRI was similar between the two groups (75.0% in the SF group and 72.7% in the NSF group, $p = 0.816$). However, the NSF group had a significantly higher number of implanted electrodes ($p = 0.025$). Focal cortical dysplasia (FCD) □ was the most common pathological finding, occurring in 34.1% of patients. Among those with malformations of cortical development (MCD) other than FCD □ (19.5% of patients), 11 had FCD I, 3 had tuberous sclerosis complex, 1 had FCD □c, and 1 had a mild malformation of cortical development with oligodendroglial hyperplasia and epilepsy. Patients with FCD □a were included in the hippocampal sclerosis (HS) group. We observed a significant difference in the pathological findings between the SF and NSF groups ($p = 0.014$), particularly between FCD □ and gliosis/non-specific findings.

Morphology, Distribution and Parameters of Ictal Harmonic Pattern

We summarized the morphological characteristics of the ictal *H* pattern in patients who exhibited only one type of *H* pattern in **Table S2**. The most frequently observed

shapes were the declining line (57.3%) and the parabola (40.2%) (**Figure S2**). Our analysis revealed no correlation between the clarity or shape of the *H* pattern and clinical factors, including the presence of lesional MRI findings, focal-onset pattern, neocortical epilepsy, pathology, or surgical outcome.

Out of 85 patients with focal-onset patterns, we identified both the SOZ and the PZ in 65 patients. Within these zones, the proportion of channels exhibiting the ictal *H* pattern was significantly higher in the SOZ (100.0%, IQR 57.3-100%) compared to the PZ (26.3%, IQR 0-50.0%; $p < 0.0001$) (**Figure 2A**). Similarly, the ictal d*H* pattern appeared more frequently in the SOZ (38.5%, IQR 16.0-80.0%) than in the PZ (0%, IQR 0-5.8%; $p < 0.0001$) (**Figure 2A**). The ictal *H* pattern was less common in other regions, and we did not observe a significant difference in the distribution of the non-d*H* pattern between the SOZ and PZ. Among the 65 patients, 37 exhibited the ictal *H* pattern simultaneously in both the SOZ and PZ. The number of frequency bands of the ictal *H* pattern was notably higher in the SOZ (3.1, IQR 2.2-6.2) compared to the PZ (2.5, IQR 1.9-4.2; $p < 0.0001$), as was the maximal frequency (SOZ, 118.8, IQR 92.5-333.0 Hz; PZ, 90.0, IQR 66.3-112.6 Hz; $p < 0.0001$). The onset time of the ictal *H* pattern did not differ between the SOZ and PZ, indicating almost simultaneous initiation across these regions. Furthermore, we did not observe differences in the termination, fundamental frequency, or frequency interval of the ictal *H* pattern between the SOZ and PZ (**Figure 2B-D**). These parameters of the ictal *H* pattern also did not differ between the SF and NSF groups (**Figure 3B-E**). In the remaining 20 patients without a PZ, the d*H* pattern was predominantly expressed in 88.9% of channels within the SOZ (IQR, 54.6-88.9%) and was rarely observed in other regions.

Ictal Dominant Harmonic Pattern

Figure 3A shows that a higher removal ratio of the $Channel_{dH\ pattern}$ significantly correlates with achieving seizure freedom ($p = 0.014$). The SF group demonstrated a

higher removal ratio of the $Channel_{dH\ pattern}$ within non-SOZ (100.0, IQR 100-100%) compared to the NSF group (100.0, IQR 0-100%; $p = 0.036$).

Predictive Value of Removing Ictal Dominant Harmonic Pattern

Regression analysis identified several independent factors significantly associated with achieving seizure freedom. These factors include the complete removal of the $Channel_{dH\ pattern}$ ($p = 0.022$; OR 6.035, 95% CI 1.291-28.211), FCD □ or other MCD types (as opposed to gliosis or other non-specific pathologies), and a smaller number of implanted electrodes (**Figure 4**). Additionally, the association between the complete removal of the $Channel_{dH\ pattern}$ and seizure freedom was supported by an analysis showing statistical significance ($p = 0.031$, AUC = 0.606) (**Figure 5**). The highest AUC value of 0.660 was recorded when considering the complete removal of the $Channel_{dH\ pattern}$ within non-SOZ, highlighting the importance of the ictal d*H* pattern for localizing the EZ (**Figure S3)**.

Survival Analysis

Figure 6 and **Figure S4** illustrate the 10-year prognosis of seizure freedom for patients who underwent *complete removal* (100%) compared to those with *incomplete* or *no removal* (0~100%). Among the 85 patients in the cohort, 58.2% achieved seizure freedom at the 10-year mark. Notably, patients who underwent complete removal of the $Channel_{dH\ pattern}$ had a significantly higher probability of attaining long-term seizure freedom ($p = 0.008$). Specifically, among the 37 patients with complete removal of the $Channel_{dH\ pattern}$ within non-SOZ, there was also an increased likelihood of achieving seizure freedom ($p = 0.028$). In cases of neocortical epilepsy, the complete removal of the $Channel_{dH\ pattern}$ was strongly associated with long-term seizure freedom (p=0.0004), regardless of whether the removal occurred within the SOZ ($p = 0.013$) or non-SOZ ($p = 0.011$) (**Figure S5**). In contrast, for mesial temporal lobe epilepsy (mTLE), complete removal of the SOZ, rather than the $Channel_{dH\ pattern}$,

was significantly associated with better long-term seizure freedom outcomes (p = 0.019).

Discussion

The ictal *H* pattern, which reflects the non-linear features of ictal SEEG signals on TF maps, may serve as an innovative ictal biomarker and offer a new approach for delineating the boundary of the EZ. Our key findings reveal: (1) In patients with focal onset patterns, the morphology of the ictal *H* pattern is consistent within individuals but heterogeneous across the cohort; (2) the morphological features of the ictal *H* pattern do not correlate with clinical variables; (3) the dominance of the ictal *H* pattern indicates high epileptogenicity, and removing regions that exhibit this pattern is crucial for achieving seizure freedom in focal epilepsy, particularly in neocortical epilepsy.

Previous studies have introduced various quantitative biomarkers for measuring spectral components of SEEG signals, including EI [7, 22], HFOs [23], and ictal non-linear metrics such as the h^2 coefficient [24, 25], coherence analysis [26, 27], entropy [28, 29], and infraslow activity [30-32]. These computational EEG markers aim to enhance the precision of EZ delineation. Our findings suggest that the ictal d*H* pattern could be a valuable biomarker for localizing the core epileptogenic cortex across different brain regions. Visual inspection showed that the distribution of the ictal *H* pattern aligned with the ictal onset zone, regardless of whether it was focal-, multifocal-, or diffuse-onset. In individuals with focal-onset patterns, the ictal *H* pattern typically exhibited a consistent spatial distribution across various seizures. In contrast, individuals with non-focal onset patterns displayed variable types of the ictal *H* pattern, indicating an unstable seizure propagation pattern. The near-simultaneous onset of the ictal *H* pattern across different regions, along with a uniform fundamental frequency, suggests clear inter-regional synchronization during this period. Notably, our findings indicate that regions showing the d*H* pattern can extend into the PZ beyond the boundary of the SOZ. As our previous research indicated, the *H* pattern

reflects spectral skewness or asymmetry in EEG waveforms, and the d*H* pattern represents stronger inter-regional synchronization during seizure evolution, particularly in focal epilepsy. These findings further support the utility of the d*H* pattern as a non-linear feature in delineating the EZ. Future clinical practices in defining the EZ would benefit from incorporating an integrated EEG biomarker that includes analysis of the d*H* pattern.

We analyzed the morphological features of the *H* pattern in terms of shape and clarity. The shape of the spectral bands in the *H* pattern reflects variations in the frequency of synchronized neural oscillations. The most frequently observed shape is a declining line, which closely resembles a spectral signature known as *chirps* [33-35]. This shape may indicate a decline in neural firing, possibly due to increased inhibition. In our cohort, nearly half of the SOPs exhibiting low-frequency activity (LVFA) expressed *chirp* [13] patterns, with proportions similar to those of the parabolic shape. We propose that some *H* patterns with a parabolic shape and very short upward lines might be classified as chirps due to the limitations of visual inspection. This potential misclassification could narrow the scope of the ictal *H* pattern and limit its applicability. A corticothalamic computational model has similarly elucidated how changes in physiological parameters affect the dynamics of tonic-clonic seizures, similar to the *H* pattern. This model revealed that increasing the connection strength enhances the power, count, and duration of harmonic bands [36]. Conversely, the clarity of the *H* pattern signifies the distinctness of the harmonic signals against the background. A highly clear *H* pattern is characterized by a narrow frequency band with minimal noise. Interestingly, these morphological properties do not correlate with clinical factors such as seizure-onset pattern, seizure origin, MRI findings, pathological findings, or seizure outcome. The primary clinically relevant aspect of the *H* pattern is its degree of non-linearity. Regardless of its shape, the prominence of the *H* pattern indicates epileptogenicity, and its complete removal has been linked to the potential achievement of seizure freedom.

We observed a stronger association between the d*H* pattern and long-term seizure

freedom in neocortical epilepsy compared to mTLE. Previous studies have reported that patients with mTLE generally experience more favorable surgical outcomes than those with neocortical epilepsy [37]. Additionally, the classification of seizure outcomes can vary among patients. Therefore, we used Engel class Ia as the criterion for a favorable outcome to evaluate the efficacy of the d*H* pattern in localizing the EZ. Earlier iEEG studies have indicated that the extent of SOZ removal does not always correlate with seizure freedom across all patients [38, 39]. In contrast, we found that, for mTLE, the complete removal of the SOZ had a stronger correlation with long-term seizure freedom than the d*H* pattern. Furthermore, our current mTLE cohort included more MRI-negative cases compared to our previous cohort [14]. Surgical outcomes in MRI-negative cases are usually less favorable compared to those in TLE-HS [40, 41], suggesting a more extensive epileptogenic network in MRI-negative TLE. Previous research has highlighted differences in the involved neural networks between mTLE and neocortical epilepsy. For instance, an ^{18}F-FDG-PET study revealed distinct metabolic profiles between these two types of epilepsy, suggesting variations in seizure propagation [42]. Additionally, an iEEG study showed that the interictal epileptogenic network in mTLE exhibits a more regular pattern of graph connectivity compared to neocortical epilepsy [43]. It is well-recognized that epileptic networks differ between mTLE and neocortical temporal lobe epilepsy, as well as between TLE and extra-TLE [44, 45]. A longer follow-up period is necessary to assess the final prognosis in patients with mTLE and to further estimate the value of the *H* pattern in this population.

Nevertheless, our study has several limitations. First, we based the determination of the *H* pattern's dominance solely on visual interpretation throughout the study. Future investigations should focus on optimizing the definition of the d*H* pattern and developing a more automated algorithm to quantify the *H* pattern. This would enhance the precision and objectivity of the analysis. We plan to create a quantitative index for the *H* pattern to address this issue. Additionally, we did not analyze the occurrence of the second *H* pattern during the later ictal stage of one seizure in this

study, which warrants further investigation.

Conclusions

In focal epilepsy, the dominance of the ictal *H* pattern offers new insights for localizing the EZ, regardless of its morphology. The distinct non-linear feature of the H pattern has significant implications for presurgical assessments and surgical planning. Applying this biomarker in neocortical epilepsy may offer greater value in achieving long-term favorable outcomes compared to mTLE.

Data availability

The that support the findings of this study are available upon reasonable request from the corresponding author.

Acknowledgements

This study received support from the National Natural Science Foundation of China (grant number: 82171437, 82301636, 82471469) and the Major Program of the National Natural Science Foundation of Zhejiang Province (grant number: LD24H090003).

Disclosures

The authors have no conflicts of interest to disclose related to this study.

Supplementary material

Supplementary material is available online.

References

1. Cardinale F, Rizzi M, Vignati E, et al. Stereoelectroencephalography: retrospective analysis of 742 procedures in a single centre. Brain 2019;142:2688-2704.

2. Jehi L, Morita-Sherman M, Love TE, et al. Comparative Effectiveness of Stereotactic Electroencephalography Versus Subdural Grids in Epilepsy Surgery. Ann Neurol 2021;90:927-939.

3. Sivaraju A, Hirsch L, Gaspard N, et al. Factors Predicting Outcome After Intracranial EEG Evaluation in Patients With Medically Refractory Epilepsy. Neurology 2022;99:e1-e10.

4. Vakharia VN, Duncan JS, Witt JA, Elger CE, Staba R, Engel J, Jr. Getting the best outcomes from epilepsy surgery. Ann Neurol 2018;83:676-690.

5. Rosenow F, Lüders H. Presurgical evaluation of epilepsy. Brain 2001;124:1683-1700.

6. Widjaja E, Li B, Schinkel CD, et al. Cost-effectiveness of pediatric epilepsy surgery compared to medical treatment in children with intractable epilepsy. Epilepsy Res 2011;94:61-68.

7. Bartolomei F, Chauvel P, Wendling F. Epileptogenicity of brain structures in human temporal lobe epilepsy: a quantified study from intracerebral EEG. Brain 2008;131:1818-1830.

8. David O, Blauwblomme T, Job AS, et al. Imaging the seizure onset zone with stereo-electroencephalography. Brain 2011;134:2898-2911.

9. Ochi A, Otsubo H, Donner EJ, et al. Dynamic changes of ictal high-frequency oscillations in neocortical epilepsy: using multiple band frequency analysis. Epilepsia 2007;48:286-296.

10. Modur PN, Zhang S, Vitaz TW. Ictal high-frequency oscillations in neocortical epilepsy: implications for seizure localization and surgical resection. Epilepsia 2011;52:1792-1801.

11. Fujiwara H, Greiner HM, Lee KH, et al. Resection of ictal high-frequency

446 oscillations leads to favorable surgical outcome in pediatric epilepsy. Epilepsia
447 2012;53:1607-1617.
448 12. Grinenko O, Li J, Mosher JC, et al. A fingerprint of the epileptogenic zone in
449 human epilepsies. Brain 2018;141:117-131.
450 13. Di Giacomo R, Burini A, Chiarello D, et al. Ictal fast activity chirps as markers of
451 the epileptogenic zone. Epilepsia 2024;65:e97-e103.
452 14. Lingli H, Lingqi Y, Hongyi Y, et al. Harmonic patterns embedding ictal EEG
453 signals in focal epilepsy: a new insight into the epileptogenic zone. medRxiv
454 2024:2023.2012.2020.23300274.
455 15. Hu L, Xiong K, Ye L, et al. Ictal EEG desynchronization during low-voltage fast
456 activity for prediction of surgical outcomes in focal epilepsy. J Neurosurg 2022:1-10.
457 16. Tadel F, Baillet S, Mosher JC, Pantazis D, Leahy RM. Brainstorm: a user-friendly
458 application for MEG/EEG analysis. Comput Intell Neurosci 2011;2011:879716.
459 17. Engel J. Outcome with respect to epileptic seizures. 1993.
460 18. Wang S, So NK, Jin B, et al. Interictal ripples nested in epileptiform discharge
461 help to identify the epileptogenic zone in neocortical epilepsy. Clin Neurophysiol
462 2017;128:945-951.
463 19. Bernardino A, Santos-Victor J. A Real-Time Gabor Primal Sketch for Visual Attention.
464 2005; Berlin, Heidelberg: Springer Berlin Heidelberg: 335-342.
465 20. Thomson DJ. Spectrum estimation and harmonic analysis. Proceedings of the
466 IEEE 1982;70:1055-1096.
467 21. Babadi B, Brown EN. A review of multitaper spectral analysis. IEEE Trans
468 Biomed Eng 2014;61:1555-1564.
469 22. Aubert S, Wendling F, Regis J, et al. Local and remote epileptogenicity in focal
470 cortical dysplasias and neurodevelopmental tumours. Brain 2009;132:3072-3086.
471 23. González Otárula KA, von Ellenrieder N, Cuello-Oderiz C, Dubeau F, Gotman J.
472 High-Frequency Oscillation Networks and Surgical Outcome in Adult Focal Epilepsy.
473 Ann Neurol 2019;85:485-494.
474 24. Bartolomei F, Lagarde S, Wendling F, et al. Defining epileptogenic networks:

475 Contribution of SEEG and signal analysis. Epilepsia 2017;58:1131-1147.
476 25. Hu L, Xiong K, Ye L, et al. Ictal EEG desynchronization during low-voltage fast
477 activity for prediction of surgical outcomes in focal epilepsy. J Neurosurg
478 2023;139:238-247.
479 26. Li YH, Ye XL, Liu QQ, et al. Localization of epileptogenic zone based on graph
480 analysis of stereo-EEG. Epilepsy Res 2016;128:149-157.
481 27. Ren Y, Cong F, Ristaniemi T, Wang Y, Li X, Zhang R. Transient seizure onset
482 network for localization of epileptogenic zone: effective connectivity and graph
483 theory-based analyses of ECoG data in temporal lobe epilepsy. J Neurol
484 2019;266:844-859.
485 28. Travnicek V, Klimes P, Cimbalnik J, et al. Relative entropy is an easy-to-use
486 invasive electroencephalographic biomarker of the epileptogenic zone. Epilepsia
487 2023;64:962-972.
488 29. Bratu IF, Makhalova J, Garnier E, et al. Permutation entropy-derived parameters
489 to estimate the epileptogenic zone network. Epilepsia 2023.
490 30. Rodin E, Modur P. Ictal intracranial infraslow EEG activity. Clin Neurophysiol
491 2008;119:2188-2200.
492 31. Kanazawa K, Matsumoto R, Imamura H, et al. Intracranially recorded ictal direct
493 current shifts may precede high frequency oscillations in human epilepsy. Clin
494 Neurophysiol 2015;126:47-59.
495 32. Nakatani M, Inouchi M, Daifu-Kobayashi M, et al. Ictal direct current shifts
496 contribute to defining the core ictal focus in epilepsy surgery. Brain Commun
497 2022;4:fcac222.
498 33. Schiff SJ, Colella D, Jacyna GM, et al. Brain chirps: spectrographic signatures of
499 epileptic seizures. Clin Neurophysiol 2000;111:953-958.
500 34. Breakspear M, Roberts JA, Terry JR, Rodrigues S, Mahant N, Robinson PA. A
501 unifying explanation of primary generalized seizures through nonlinear brain
502 modeling and bifurcation analysis. Cereb Cortex 2006;16:1296-1313.
503 35. Dutta S, Iyer KK, Vanhatalo S, Breakspear M, Roberts JA. Mechanisms
504 underlying pathological cortical bursts during metabolic depletion. Nat Commun

505 2023;14:4792.
506 36. Deeba F, Sanz-Leon P, Robinson PA. Effects of physiological parameter
507 evolution on the dynamics of tonic-clonic seizures. PLoS One 2020;15:e0230510.
508 37. Spencer S, Huh L. Outcomes of epilepsy surgery in adults and children. Lancet
509 Neurol 2008;7:525-537.
510 38. Khan M, Chari A, Seunarine K, et al. Proportion of resected seizure onset zone
511 contacts in pediatric stereo-EEG-guided resective surgery does not correlate with
512 outcome. Clin Neurophysiol 2022;138:18-24.
513 39. Thomas J, Kahane P, Abdallah C, et al. A Subpopulation of Spikes Predicts
514 Successful Epilepsy Surgery Outcome. Ann Neurol 2023;93:522-535.
515 40. Fong JS, Jehi L, Najm I, Prayson RA, Busch R, Bingaman W. Seizure outcome
516 and its predictors after temporal lobe epilepsy surgery in patients with normal MRI.
517 Epilepsia 2011;52:1393-1401.
518 41. McIntosh AM, Wilson SJ, Berkovic SF. Seizure outcome after temporal
519 lobectomy: current research practice and findings. Epilepsia 2001;42:1288-1307.
520 42. Zhu HY, Tang YX, Xiao L, et al. Metabolic profiles and correlation with surgical
521 outcomes in mesial versus neocortical temporal lobe epilepsy. CNS Neurosci Ther
522 2023;29:2656-2665.
523 43. Bartolomei F, Bettus G, Stam CJ, Guye M. Interictal network properties in mesial
524 temporal lobe epilepsy: a graph theoretical study from intracerebral recordings. Clin
525 Neurophysiol 2013;124:2345-2353.
526 44. González Otárula KA, Schuele S. Networks in Temporal Lobe Epilepsy.
527 Neurosurg Clin N Am 2020;31:309-317.
528 45. Hall GR, Hutchings F, Horsley J, et al. Epileptogenic networks in extra temporal
529 lobe epilepsy. Netw Neurosci 2023;7:1351-1362.
530

Figure Legends

Figure 1. Examples and characteristics of the *H* pattern (data from patient #057). (A) Ictal SEEG recordings from both SOZ and PZ of a patient with right parietal focal cortical dysplasia showing bursts of high-amplitude poly-spikes followed by low-voltage fast activity at seizure onset. Below the SEEG recordings are corresponding time-frequency plots of the two channels. An ictal *H* pattern could be identified in both plots: two or more unique high-intensity spectral bands with varying frequency starting at 4 s (red arrow) after 0 s (seizure onset), and ending at 19 s (red arrow). The frequencies of the bottom and top spectral bands are defined as the *fundamental frequency* and *maximal frequency*, respectively (yellow arrow). Importantly, the ictal *H* pattern exhibits a distinctive feature of equidistant distribution on the TF plots. For instance, at 6.3 s (long blue dotted arrows), the frequency interval between adjacent spectral bands is nearly uniform, at approximately 26-28 Hz, as observed in the power spectral density diagrams. The ictal *H* pattern shown in the two channels are classified as a 'dominant *H* pattern (d*H* pattern)' and a 'non-dominant *H* pattern (non-d*H* pattern)', respectively. (B) 3D representation of an example SEEG exploration. Electrode contacts are categorized into three regions: the SOZ (red dots), the PZ (orange dots), and the other regions (blue dots), according to a patient's ictal SEEG recordings. (C) Total number of visually determined spectral bands on the TF plot of each channel each time a seizure is counted. Channels are then ranked based on the number of bands, and if a channel's count exceeds the threshold of *Q3*, it is marked as expressing the ictal dominant *H* pattern. SEEG, stereo-electroencephalography; SOZ, seizure-onset zone; PZ, early propagation zone; *H* pattern, *Harmonic* pattern; *Q3*, the 75th percentile of data distribution.

Figure 2. Distribution and time-frequency features of ictal *H* patterns in SOZ and PZ. (A) Proportions of channels expressing the ictal *H* pattern, the ictal dominant *H* pattern, and the ictal non-dominant *H* pattern between SOZ (red dots) and PZ (orange dots) in 65 patients who had both SOZ and PZ. (B-F) Onset and end time,

560 fundamental frequency, maximal frequency, frequency interval, and number of
561 spectral bands of the ictal *H* pattern between SOZ and PZ in 37 patients that
562 simultaneously expressed the ictal *H* pattern in both SOZ and PZ.
563 ****: $p < 0.0001$, nonparametric Mann-Whitney U test; *H* pattern, *Harmonic* pattern;
564 SOZ, seizure-onset zone; PZ, early propagation zone.
565
566 **Figure 3. Associations between proportions of removal, time-frequency features**
567 **of the ictal *H* patterns, and seizure outcomes.** (A) Violin diagrams comparing
568 removed ratios in channels of SOZ, channels expressing the ictal *H* pattern, channels
569 expressing the ictal dominant *H* pattern, and channels expressing the ictal
570 non-dominant *H* pattern between seizure-free (blue hollow circles) and not
571 seizure-free (red hollow triangles) patients. (B-E) Onset time, end time, fundamental
572 frequency, maximal frequency, frequency interval, and the number of spectral bands
573 of the ictal *H* pattern between seizure-free (blue dots) and not seizure-free (red dots)
574 patients. *H pattern*, *Harmonic* pattern; SOZ, seizure-onset zone.
575
576 **Figure 4. Binary regression for classification of seizure outcomes.** Seven variables
577 were recruited into the equation: EEG pattern harboring the *H* pattern, lesional MRI
578 findings, seizure localization (mesial temporal lobe or neocortex), pathological
579 findings, removed ratios of channels of the seizure-onset zone, channels expressing
580 the ictal *H* pattern, and channels expressing the ictal dominant *H* pattern. The forest
581 plot shows complete removal of channels expressing the ictal dominant *H* pattern,
582 FCD type-II, or other MCD types (compared to gliosis/other non-specific pathology).
583 Less implanted electrodes were correlated with seizure freedom. EEG,
584 electroencephalography; *H* pattern, *Harmonic* pattern; MRI, magnetic resonance
585 imaging; FCD, focal cortical dysplasia; MCD, malformation of cortical development;
586 OR, odds ratio; CI, confidence interval.
587
588 **Figure 5. Predictive values for seizure outcomes.** (A-D) Four-fold tables and
589 receiver operator characteristic curve (ROC) for the removed ratios of channels within

the seizure-onset zone (dark red), channels expressing the ictal *H* pattern (orange), channels expressing the ictal dominant *H* patten (scarlet), and channels expressing the ictal non-dominant *H* pattern (yellow) as predictors of post-surgical outcomes. In the four-fold tables, the numbers of seizure-free patients and not seizure-free patients with all the corresponding channels removed ('*Yes*', upper left of the table), or incompletely/none removed ('*No*', bottom left of the table) are listed. *p*-values for each *Chi-Squared* test are provided above each table. In the ROC curves, each colored dot represents a combined value of the false positive rate (X-axis) and the true positive rate (Y-axis). The areas under curves (AUCs) are respectively listed on the bottom right corner.

Figure 6. Survival analysis. Kaplan-Meier (KM) plots of cumulative probability of continuous seizure freedom separated by complete (100%) removal (green continuous line) and incomplete/none (0~100%) removal (blue continuous line) of the whole cohort, channels of seizure-onset zone, channels expressing the ictal *H* pattern, channels expressing the ictal dominant *H* patten, and channels expressing the ictal non-dominant *H* pattern. The ‘number at risk (number censored)’ of each year is annotated below the KM plot for every category.

Table 1. Patients' demographics and surgical outcome

	Total cohort	Seizure-free (Engel class Ia)	Non-seizure free (> Engel class Ia)	*p* value
Number of patients, n	85	52	33	-
Gender, M, n (%)	47 (55.3%)	29 (55.8%)	18 (54.5%)	0.912[a]
Age at onset, y	10.0 (6.0-15.4)	8.5 (5.8-18.8)	12.0 (6.5-15.4)	0.338[c]
Age at SEEG recording, y	23.3 ± 10.4	23.0 ± 11.1	23.7 ± 9.4	0.753[b]
EEG pattern at *H* pattern, n (%)				
Irregular spiking (IS)	29 (34.1%)	17 (32.7%)	12 (36.4%)	0.728[a]
Fast activity (FA)	56 (65.9%)	35 (67.3%)	21 (63.6%)	
Lateralization, n (%)				
Left	36 (42.4%)	21 (40.4%)	18 (54.5%)	0.645[a]
Right	49 (57.6%)	31 (59.6%)	15 (45.5%)	
Localization, n (%)				
Mesial temporal lobe	28 (32.9%)	15 (28.8%)	13 (39.4%)	0.313[a]
Neocortex	57 (67.1%)	37 (71.2%)	20 (60.6%)	
Lesional MRI, n (%)	63 (74.1%)	39 (75.0%)	24 (72.7%)	0.816[a]
Number of Electrodes, n	10.0 (8.0-11.5)	9.0 (7.0-11.0)	10.0 (9.0-12.5)	**0.025**[c]
Number of Contacts, n	112.0 (88.5-127.0)	112.5 (81.3-127.8)	112.0 (96.0-126.5)	0.433[c]
Bilateral implantation, n (%)	27 (31.8%)	16 (30.8%)	11 (33.3%)	0.874[a]
Pathology, n (%)	82	52	30	
Hippocampal sclerosis	13 (15.9%)	8 (15.4%)	5 (16.7%)	
FCD type-II	28 (34.1%)	22 (42.3%)[e]	6 (20.0%)[e]	
Other MCD types	16 (19.5%)	11 (21.2%)	5 (16.7%)	**0.014**[d]
Tumor	3 (3.7%)	3 (5.8%)	0	
Gliosis/other non-specific	22 (26.8%)	8 (15.4%)[f]	14 (46.7%)[f]	

Normal variables were presented as mean ± standard deviation (SD). Non-normal variables were reported as median (interquartile range, IQR). a. *Pearson's chi-square* test. b. *Unpaired t-test*. c. *Mann-Whitney U* test. d. *Fisher exact* test. e & f. *Bonferroni* correction: In the SF and NSF groups, there was a discrepancy in pathological finding (p = 0.014). A significant difference was found between FCD type-II and gliosis/non-specific findings.

SEEG, stereo-electroencephalography, H pattern, Harmonic pattern, MRI, magnetic resonance imaging, FCD, focal cortical dysplasia, MCD, malformation of cortical development

Notion: The category *Other MCD types* consists of FCD type-I, tuberous sclerosis complex, heterotopia, and mild malformation of cortical development with oligodendroglial hyperplasia in epilepsy.

Figure 1

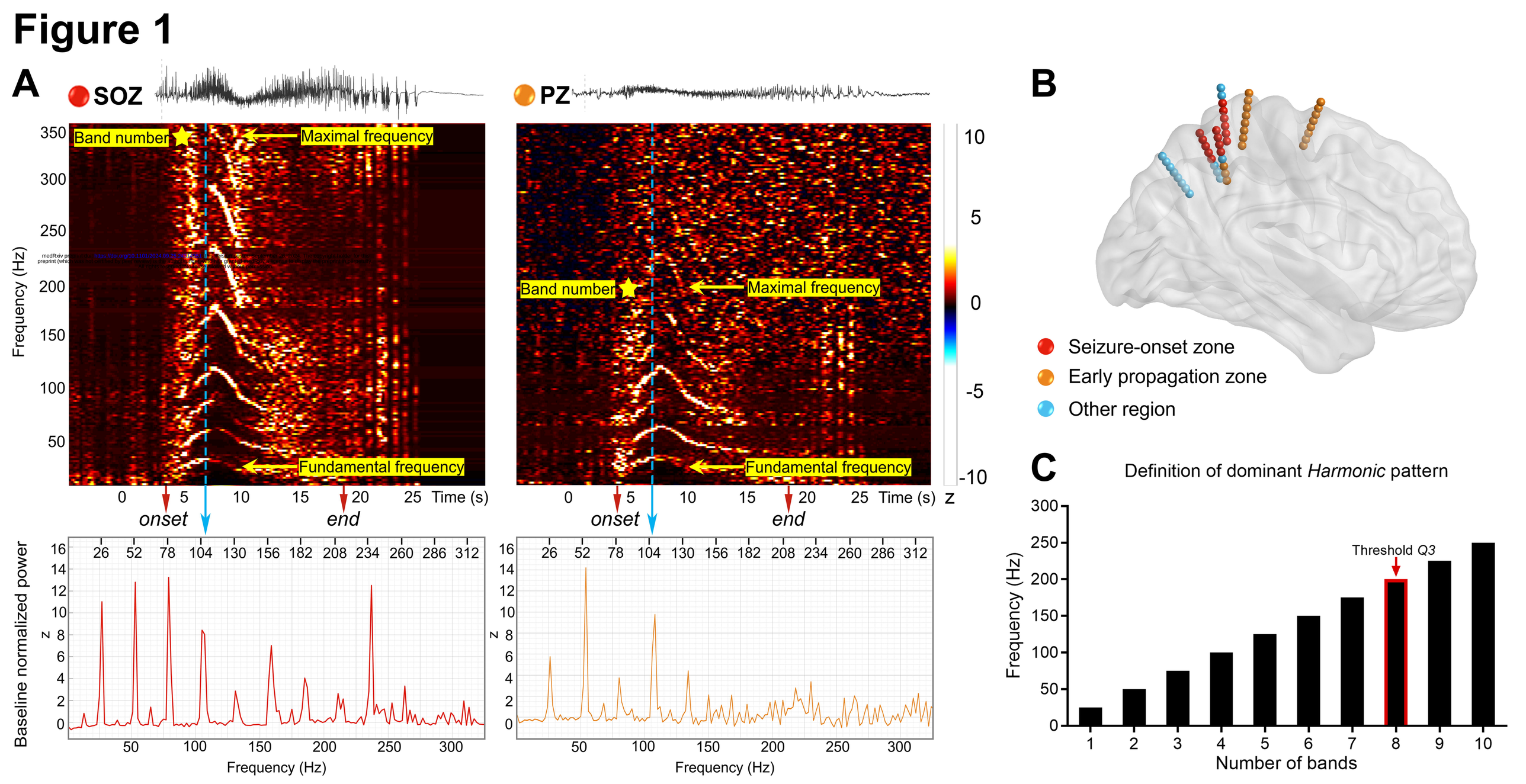
A
SOZ
PZ
Band number
Maximal frequency
Fundamental frequency
Frequency (Hz)
Time (s)
onset
end
z
Baseline normalized power
Frequency (Hz)
B
Seizure-onset zone
Early propagation zone
Other region
C
Definition of dominant Harmonic pattern
Threshold Q3
Frequency (Hz)
Number of bands

Figure 2

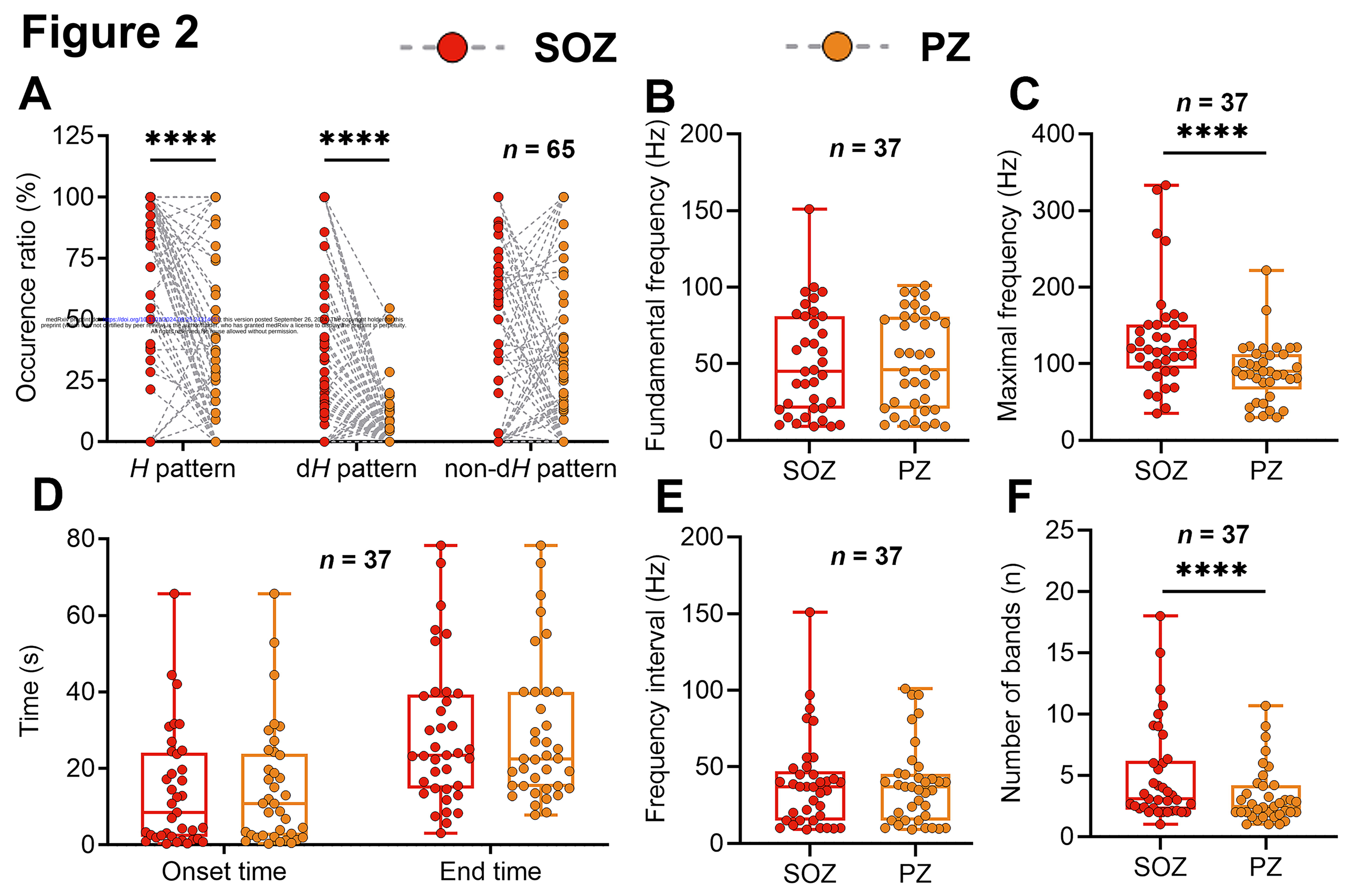

Figure 3

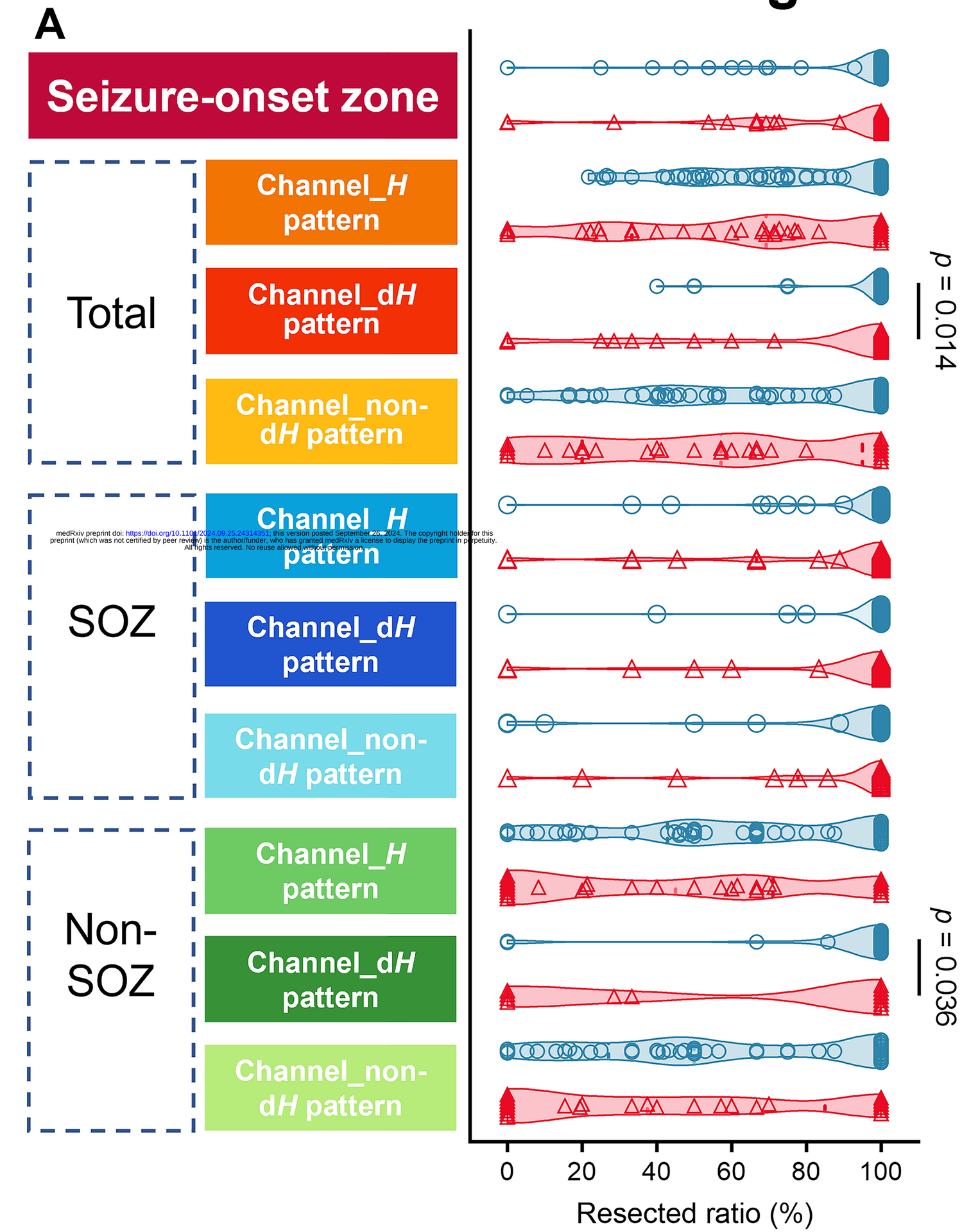

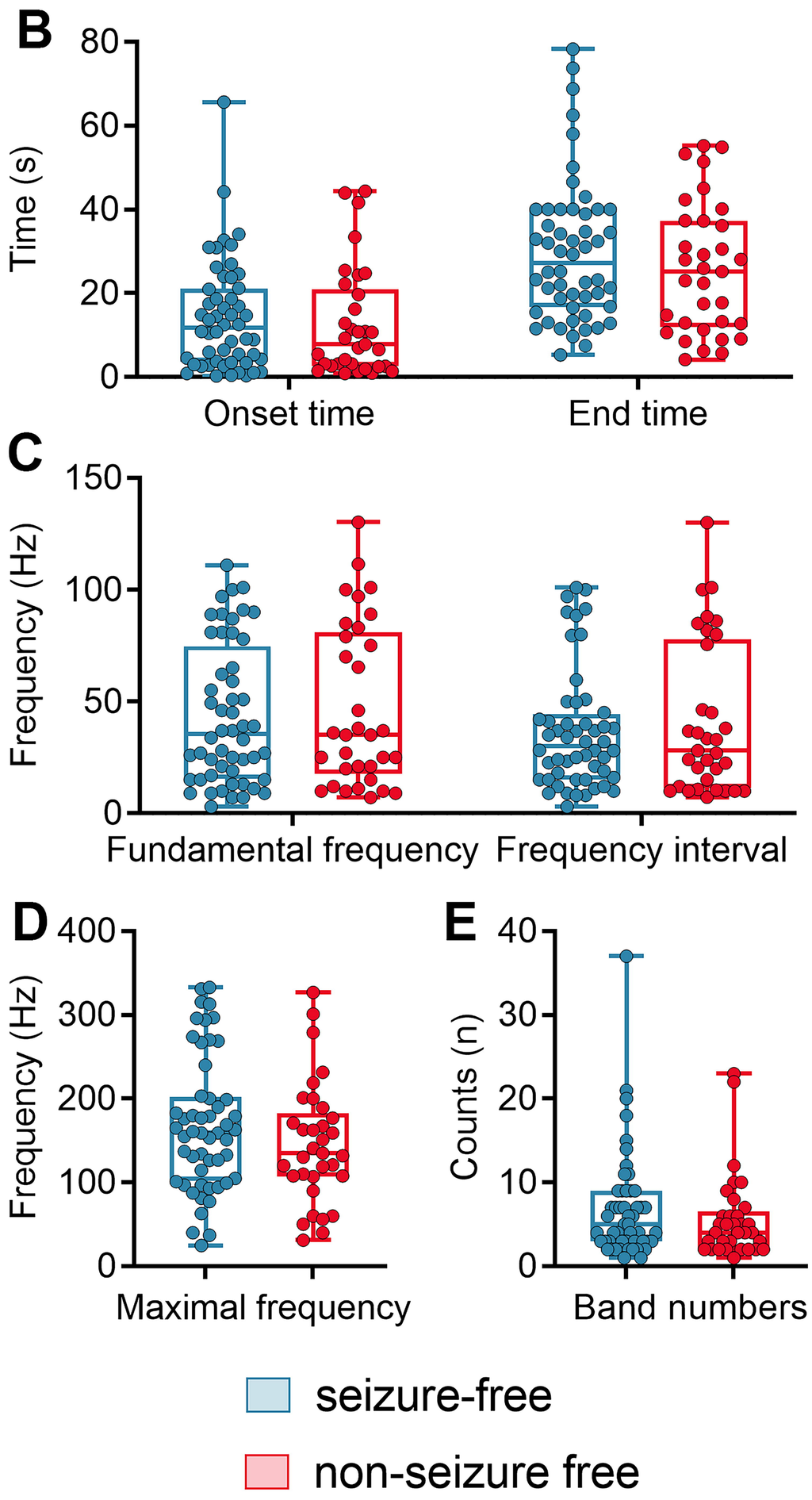

Figure 4

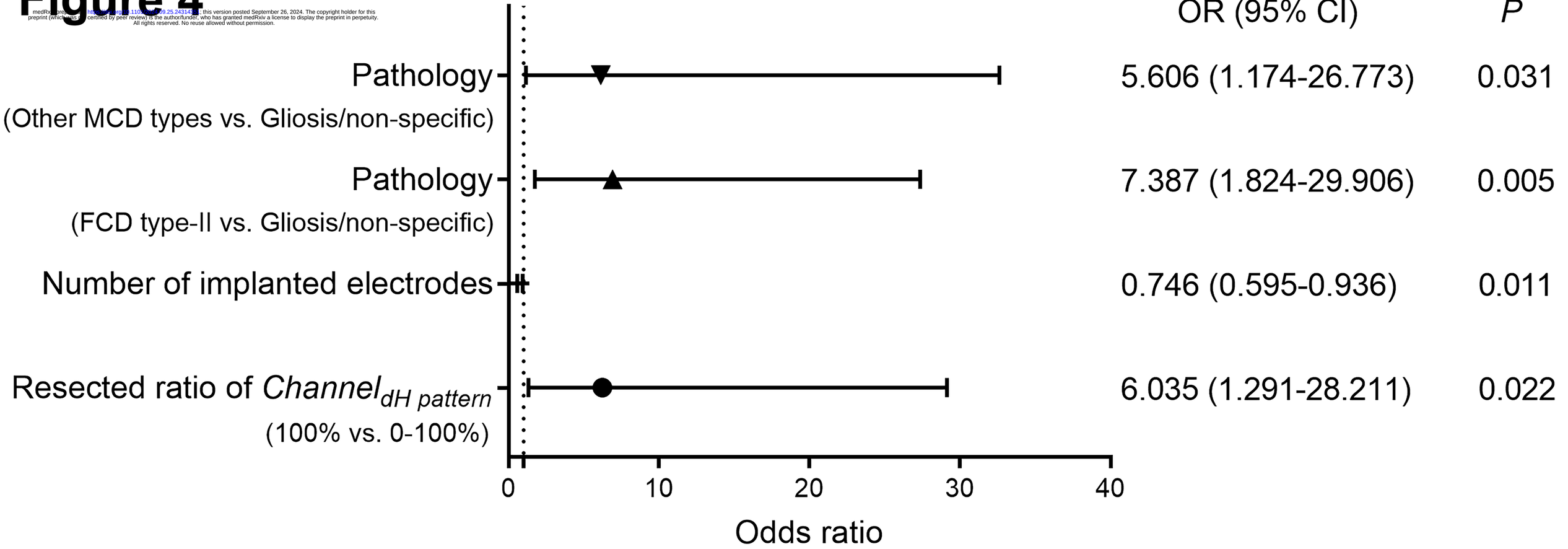

Figure 5

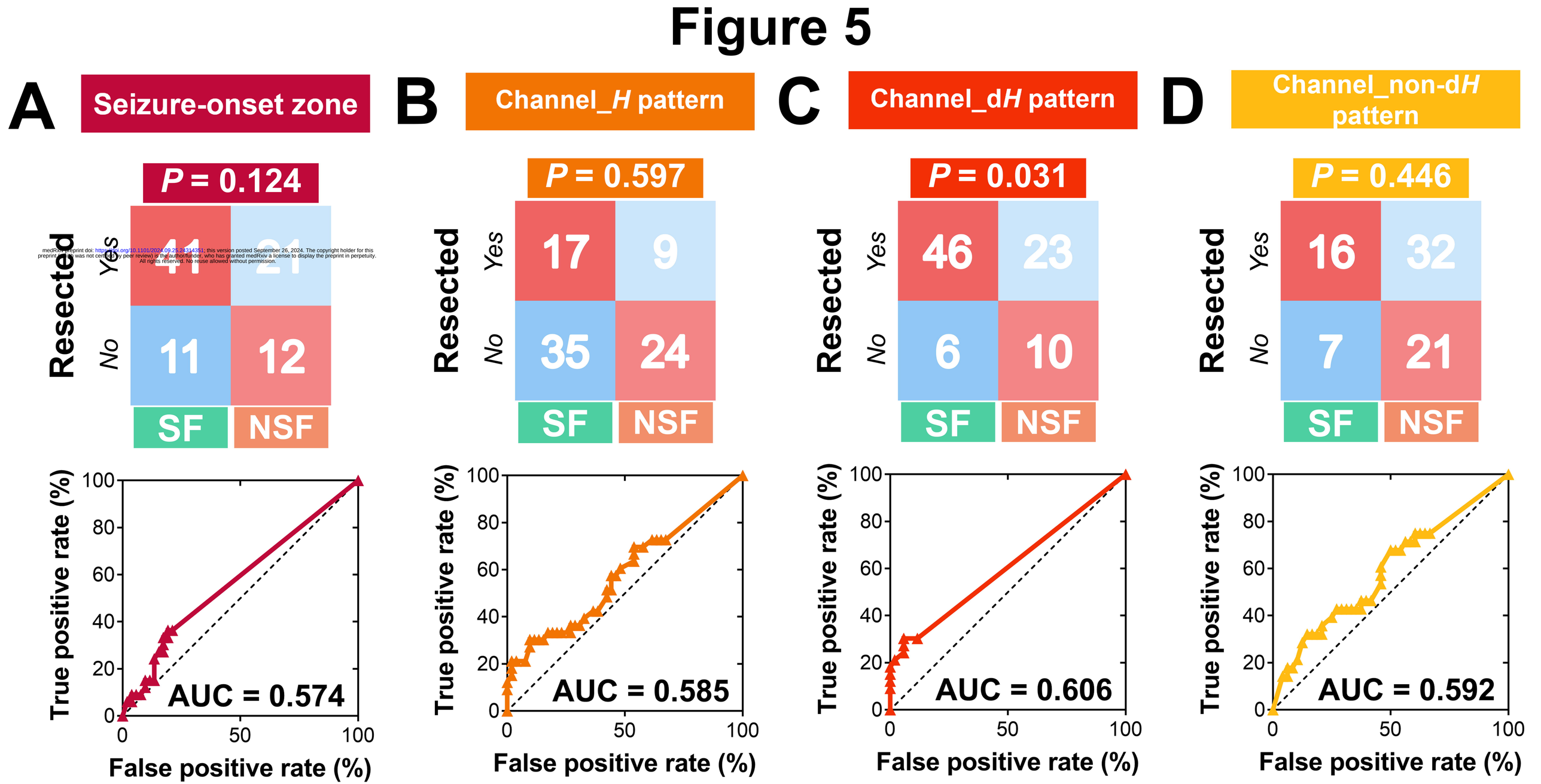

Figure 6